energies

MDPI

Article

Using Thermal Energy Storage to Relieve Wind Generation Curtailment in an Island Microgrid

Huanhuan Luo [1,2], Weichun Ge [1,2], Jingzhuo Sun [3], Quanyuan Jiang [3] and Yuzhong Gong [4,*]

1 School of Electrical Engineering, Shenyang University of Technology, Shenyang 110027, China; lhh@ln.sgcc.com.cn (H.L.); gwc@ln.sgcc.com.cn (W.G.)
2 State Grid Liaoning Electrical Power Company, Shenyang 110006, China
3 College of Electrical Engineering, Zhejiang University, Hangzhou 310027, China; jz_sun@zju.edu.cn (J.S.); jqy@zju.edu.cn (Q.J.)
4 Department of Electrical and Computer Engineering, University of Saskatchewan, Saskatoon, SK S7N 5A9, Canada
* Correspondence: y.z.gong@usask.ca

Abstract: The uncertainty and intermittency of the available wind resource in nature would potentially cause wind generation curtailment when the flexibility of the integrated power grid is limited, especially in small-scale microgrids for islands. In this paper, an optimal configuration method is proposed to use thermal energy storage (TES) to relieve wind generation curtailment in an island microgrid. The thermal network is modeled along with the electrical network to utilize its regulation capability, while TES is introduced as an additional flexibility resource. The detailed cost models of combined heat and power (CHP) units and TES are presented to realize the objective of minimizing the overall operating cost. The performance of TES in improving wind power utilization is firstly validated by using an electrical boiler (EB) as a benchmark and further analyzed under different scenarios considering the growths of wind power capacity, electrical load, and heat load. The effectiveness of the proposed method is validated using real-world data obtained from the practical island microgrid.

Keywords: island microgrid; thermal energy storage (TES); combined heat and power (CHP); wind generation curtailment

Citation: Luo, H.; Ge, W.; Sun, J.; Jiang, Q.; Gong, Y. Using Thermal Energy Storage to Relieve Wind Generation Curtailment in an Island Microgrid. *Energies* **2021**, *14*, 2851. https://doi.org/10.3390/en14102851

Academic Editor: Akhtar Kalam

Received: 29 March 2021
Accepted: 12 May 2021
Published: 15 May 2021

1. Introduction

As one of the most promising renewable power sources, wind power has been under a rapid growth in last decades. By the end of 2019, the total capacity for wind energy globally has reached 651 GW, in which China has the world's largest installed wind power capacity of 236 GW. Due to the natural intermittent property, wind power can not be dispatched on demand. When the available wind power excess the operation capability of the integrated power grid, wind curtailment has to be performed to keep power balance in the system, which leads to an critical issue of massive wind generation curtailment during the winter off-peak period in Northern China [1]. To ensure the utilization of wind power, the Government of China has also issued a set of policies to guide market design and technology development [2]. Microgrid with renewable wind power has become a popular power supply solution for islands in China [3]. As a small-scale power grid, island microgrid has a very limited operational flexibility to handle the variable wind generation, which make it more challenging to relieve wind generation curtailment.

Many research works have been conducted to relieve wind generation curtailment, such as high voltage direct current (HVDC) transmission [4], energy storage applications [5], integrated energy systems [6], and probabilistic planning and operation [7]. The thermostatically controlled loads in a microgrid are utilized in Reference [8] to mitigate the variations in renewable generation and load with a distributed control scheme. But the performance

of the solutions using demand response depends on the availability and capacity of the controllable loads. Diesel generators and battery energy storage systems (BESS) are two common options that being configured in microgrids as additional power sources and flexible resources to address the wind power integration issues. A multi-objective robust optimization model based on the information gap theory is proposed in Reference [9] to realize the island microgrid capacity configuration of diesel generators and BESS. In Reference [10], a lithium-ion BESS is designed to improve the dispatchability of uncertain renewable generation considering the degradation of battery. However, The BESS applications are restricted by the high investing cost and limited life cycles of batteries.

Integrating the electrical network and the thermal network has been proposed as another possible solution to facilitate the regulation capability of thermal network for supporting wind power utilization [11]. The combined heat and power (CHP) unit can provide electrical and heat power simultaneously and is popular in the heat-electricity integrated microgrids to facilitate energy sharing and improve system flexibility. A hybrid energy sharing framework is established for multiple microgrids in Reference [12]. However, the combined heat and power (CHP) unit has a limited operational flexibility constrained by the heat demand in winter [13]. A heavy curtailment of wind generation will be performed because a large portion of the power demand must be covered by CHP units [5].

Therefore, additional flexibility resources need to be introduced in heating supply to allow CHP units to further reduce their power output for relieving wind generation curtailment. Installing electrical boilers (EB) is one of the potential solutions that can utilize wind generation to meet the heat load demand [1]. Electrical energy storage has also been widely applied to increase the flexibility in island microgrid operation [14]. A stochastic programming framework is presented in Reference [15] for conducting optimal daily scheduling of CHP-based microgrids consisting of wind power electrical boiler, and energy storage devices. As electrical energy storage can only be dispatched to regulate electrical power network and EB can only provide one-direction flexibility, thermal energy storage (TES) is introduced as another effective solution to improve the utilization of wind generation by shifting the heating demand to off-peak hours [16,17].

A microgrid optimal dispatch with TES and demand response is proposed in Reference [18] to address the uncertainty in renewable energy. In Reference [19], an energy management system model integrating CHP units, boilers, heat pumps, and TES is built for isolated microgrid to saving daily fuel cost in winter days. An online energy management algorithm is developed in Reference [20] to minimize the microgrid's operation cost by coordinating renewable generations, CHP units, electricity and heat energy storage. However, most of studies focus on the short-term operational optimization with configured system capacities. The configuration and economic analysis of TES, combined or compared with other solutions, have not been studied in detail yet.

This work looks at a particular scenario of relieving wind generation curtailment in an island microgrid with a weak tie-line connection to external bulk grid, which has been observed in a practical island microgrid grid located in Northeast China. Considering local residential heat load in winter season, when the wind generation curtailment is a significant issue, TES is employed as an effective approach to convert and store the wind energy to satisfy heating demand. In order to achieve this goal, an extensive formulation is proposed to determine the optimal size of TES for such scenario, based on a set of detailed models of TES and CHP units. The effectiveness of the proposed approach is validated using real-world data obtained from the practical island microgrid.

The contributions of this paper include the following:

(1) The detailed technical and economic models of TES and CHP units are established to accurately describe their capabilities and costs.
(2) The thermal network is modeled along with the electrical network to utilize its regulation capability with TES being introduced as an additional flexibility resource.
(3) An optimal configuration model is proposed to determine the TES capacity for relieving wind generation curtailment while minimizing the overall operating cost.

2. Modeling of CHP Unit and TES

Figure 1 shows the structure of a microgrid consists of electrical power network and thermal energy network. The heat load is supplied by CHP units and electrical-heat conversion devices, e.g., TES or EB. The electrical load is supplied by the CHP units, wind turbines, and a tie line. The redundant wind power is used to "charge" TES within the limitation of its rated heating power.

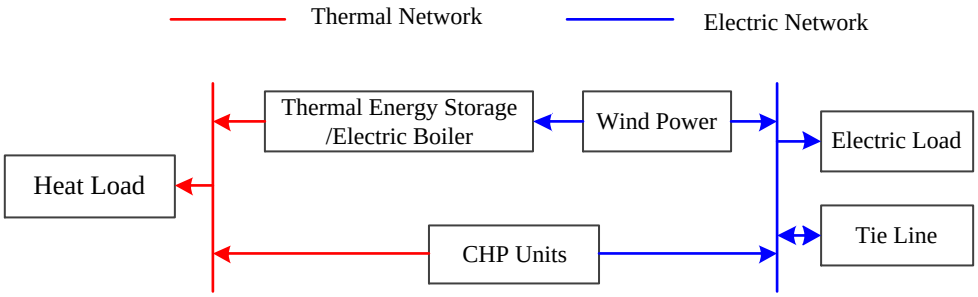

Figure 1. System structure of a microgrid integrating electrical and thermal networks.

2.1. CHP Modeling

Figure 2 illustrates the typical heat and electrical power characteristic of a CHP unit with an extraction steam turbine. Denote P_g as the active electrical power output and Q_g as the heat power output. $P_g^{\max}$ and $P_g^{\min}$ are the maximum and minimum electrical power output, while $Q_g^{\min}$ is the heat power output when $P_g = P_g^{\min}$, and $Q_g^{\max}$ is the maximum heat power output. The coefficient of electrical power and heat power under back pressure operation can be described as $c_{\mathrm{m},g} = \Delta P_g / \Delta Q_g$, which can be normally considered as a constant. ΔP_g is the power difference of P_g between point B and C in Figure 2, and ΔQ_g is the power difference of Q_g between point B and C. In other word, c_m is the slope of the line segment BC.

Denote $C_{\mathrm{v},g}$ as the reduced electrical power amount to increase per unit heat power under the same steam flow. The value of $C_{\mathrm{v},g}$ can be further defined as $C_{\mathrm{v1},g}$ under the maximum electrical power output and $C_{\mathrm{v2},g}$ under the minimum electrical power output.

As the CHP unit can generate both electricity and heat at the same time, the operating cost of a CHP unit g at time t, denoted as C_g^t, can be calculated with P_g^t and Q_g^t as

$$C_g^t = \left[b_0 + b_1 P_g^t + b_2 Q_g^t + b_3 (P_g^t)^2 + b_4 P_g^t Q_g^t + b_5 (Q_g^t)^2 \right] \cdot S_{\mathrm{coal}}, \quad (1)$$

where b_0, b_1, b_2, b_3, b_4, b_5 are the cost coefficients, and S_{coal} is the unit fuel price.

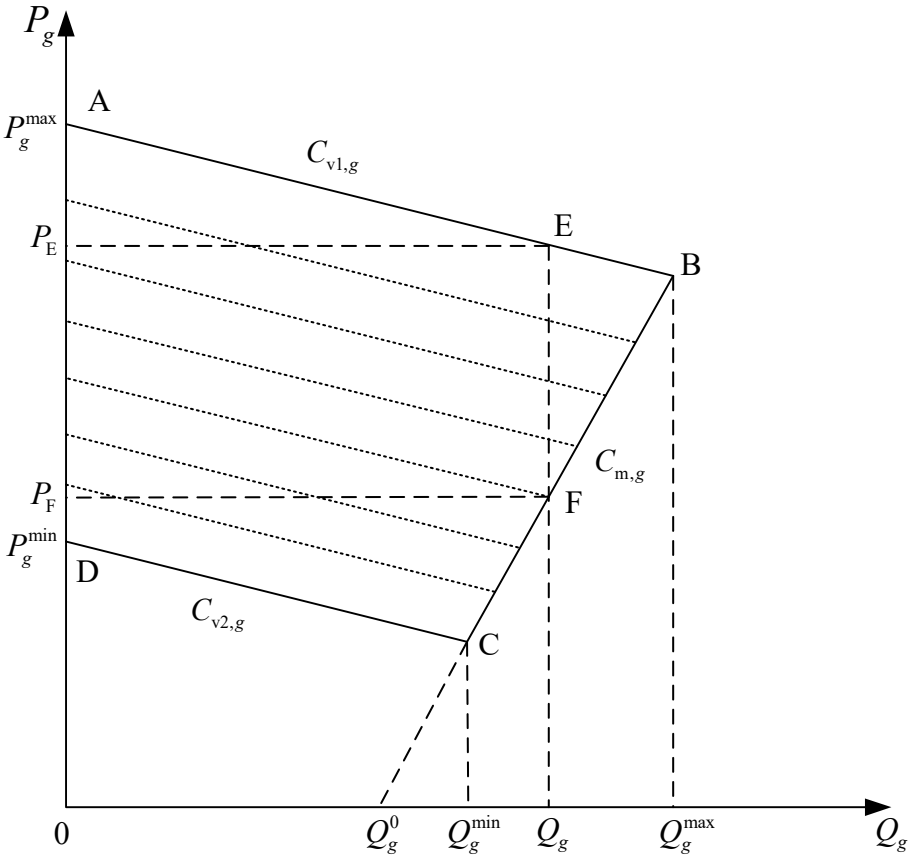

Figure 2. Electrical and heat power characteristics of CHP units.

2.2. TES Modeling

TES using phase change materials is adapted in this paper, as shown in Figure 3. The heating function of TES is realized with thermal resistance connected to a 10 kV power supply. The capital cost of TES C_n can be described with a quadratic function of the heat energy capacity $\overline{E}_{TES}$ and the rated intput heat power $\overline{P}_{TES}$ of TES.

$$C_n\left(\overline{E}_{TES}, \overline{P}_{TES}\right) = d_0 + d_1\overline{E}_{TES} + d_2\overline{E}_{TES} + d_3\overline{P}_{TES} + d_4\overline{P}_{TES}. \quad (2)$$

The operating cost of TES can be modeled with the annual depreciation cost C_a and the annual maintenance cost C_b. The former one can be obtained by projecting the capital cost can be projected into each year using the straight-line depreciation method. The latter one can be estimated as a proportion of the capital cost.

$$C_a\left(\overline{E}_{TES}, \overline{P}_{TES}\right) = C_n\left(\overline{E}_{TES}, \overline{P}_{TES}\right)\frac{\gamma(1+\gamma)^k}{(1+\gamma)^k - 1} - C_s\frac{\gamma}{(1+\gamma)^k - 1}, \quad (3)$$

$$C_b\left(\overline{E}_{TES}, \overline{P}_{TES}\right) = R_m \cdot C_n\left(\overline{E}_{TES}, \overline{P}_{TES}\right), \quad (4)$$

where γ is the annual percentage rate, C_s is the salvage value of TES, k is the service life in year, and R_m is the coefficient to estimate the maintenance cost from the capital cost.

Therefore, the overall annual operating cost of TES C_{TES} can be calculated from the annual depreciation cost and maintenance cost as

$$C_{TES}\left(\overline{E}_{TES}, \overline{P}_{TES}\right) = C_a\left(\overline{E}_{TES}, \overline{P}_{TES}\right) + C_b\left(\overline{E}_{TES}, \overline{P}_{TES}\right). \quad (5)$$

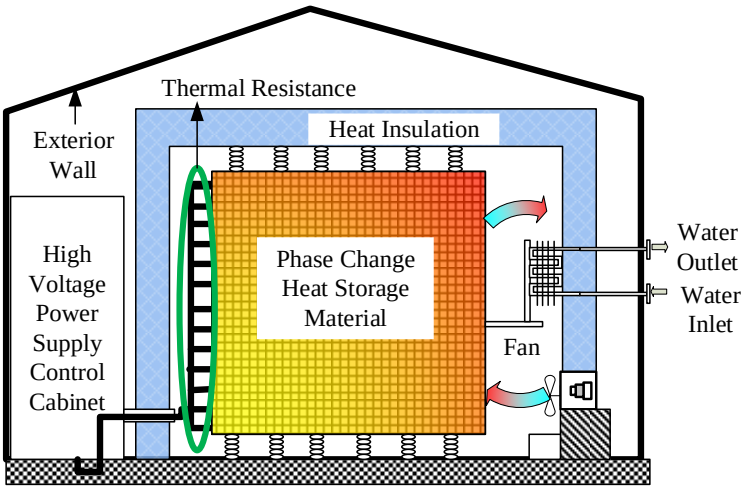

Figure 3. Schematic diagram of TES using phase change materials.

3. Configuration Method

A multi-period operational planning problem is formulated to determine the optimal size of TES to minimize the overall investing and operating costs, while utilizing the renewable wind resources as possible.

3.1. Objective Function

The objective function aims to minimize the overall cost, including the operating cost of CHP units, operating cost of wind generation, penalty of wind curtailment, cost of energy purchased through the tie line, and the annualized operating cost of TES.

$$\min \sum_{t=1}^{T} \left[\sum_{g=1}^{N_G} C_g^t \left(P_g^t, Q_g^t \right) + c_w P_w^t + c_{curt} P_{w,curt}^t + c_{tie} P_{tie}^t \right] + C_{TES} \left(\overline{E}_{TES}, \overline{P}_{TES} \right), \quad (6)$$

where T is the length of optimization horizon, N_G is the number of CHP units, C_g^t is the cost function of CHP unit g at time t, P_g^t and Q_g^t are the electrical power output and heat power output of CHP unit g at time t, c_w is the cost coefficient of wind generation in \$/MW, c_{tie} is the unit price of energy delivered through tie line, and P_{tie}^t is the exchange power of tie line at time t, P_w^t is the total wind generation at time t, c_{curt} is the penalty coefficient of wind curtailment in \$/MW, and $P_{w,curt}$ is the wind curtailment at time t, which can be calculated with the total available wind power $P_{w,avail}^t$.

$$P_{w,curt}^t = P_{w,avail}^t - P_w^t. \quad (7)$$

3.2. Operation Constraints

3.2.1. CHP Units Operation Constraints

The active electrical power output of CHP unit is restricted by both the capacity and the heat power output as

$$P_g^t \geq \min \left\{ c_{m,g} Q_g^t + K_g, P_g^{min} - c_{v2,g} Q_g^t \right\}, \quad (8)$$

$$P_g^t \leq P_g^{max} - c_{v2,g} Q_g^t, \quad (9)$$

where P_g^{min} and P_g^{max} are the minimum and maximum electrical power outputs of CHP unit g with zero heat power output, $c_{m,g}$, $c_{v1,g}$, and $c_{v2,g}$ are the values of coefficients for unit g, and K_g is a constant to describe the virtual intersection point of the segment BC and the axis of P_g in Figure 2.

Besides, P_g^t is also restricted by the ramp rate of CHP unit as

$$P_g^t - P_g^{t-1} \leq R_g^{\text{up}}, \tag{10}$$

$$P_g^{t-1} - P_g^t \leq R_g^{\text{dn}}, \tag{11}$$

where R_g^{up} and R_g^{up} are the upward and downward ramp rate limit of CHP unit g.

The heat power output of CHP unit is restricted by its heat capacity as

$$Q_g^{\min} \leq Q_g^t \leq Q_g^{\max}, \tag{12}$$

where $Q_g^{\min}$ and $Q_g^{\max}$ are the minimum and maximum heat power outputs of CHP unit g.

3.2.2. TES Operation Constraints

The input power and output power of TES are limited by its rated power capacity as

$$0 \leq P_{\text{TES}}^t \leq \overline{P}_{\text{TES}}, \tag{13}$$

$$0 \leq Q_{\text{TES}}^t \leq \overline{Q}_{\text{TES}}, \tag{14}$$

$$\overline{Q}_{\text{TES}} = 0.8 \cdot \overline{P}_{\text{TES}}, \tag{15}$$

where P_{TES}^t and Q_{TES}^t are the input and output heat power of TES at time t, and $\overline{P}_{\text{TES}}$ and $\overline{Q}_{\text{TES}}$ are the maximum input and output heat power of TES.

Considering the loss in electrical-heat conversion of TES, the electrical power required is higher than the heating power of TES.

$$P_{\text{TES}}^t = \eta_{\text{TES}} \cdot P_{\text{heat}}^t, \tag{16}$$

where P_{heat}^t is the consumed electrical power for heating TES at time t, and η_{TES} is the efficiency of electrical-heat conversion. η_{TES} is set as 0.98 in this paper.

In addition, the energy state of TES is limited by its rated energy capacity as

$$0.1\overline{E}_{\text{TES}} \leq E_{\text{TES}}^t \leq \overline{E}_{\text{TES}}, \tag{17}$$

where E_{TES}^t is the energy state of TES at time t. It can be obtained by

$$E_{\text{TES}}^t = E_{\text{TES}}^{t-1} + (P_{\text{TES}}^t - Q_{\text{TES}}^t)\Delta T, \tag{18}$$

where ΔT is the time interval.

3.2.3. EB Operation Constraints

An EB is also considered to be configured in the microgrid for heat supply using electricity, the operation of which is modelled with its rated power and efficiency as

$$0 \leq P_{\text{EB}}^t \leq \overline{P}_{\text{EB}}, \tag{19}$$

$$Q_{\text{EB}}^t = \eta_{\text{EB}} P_{\text{EB}}^t, \tag{20}$$

where P_{EB}^t is the electrical power consumption at time t, $\overline{P}_{\text{EB}}$ is the rated power of EB, Q_{EB}^t is the heat power output of EB at time t, and η_{EB} is the conversion efficiency of EB. η_{EB} is set as 0.98 in this paper.

3.2.4. Electrical Power Balance Constraints

The electrical load in the island consists of normal power load P_{eload}^t and the EB power P_{EB}^t, which is supplied by the integrated wind generation P_{w}^t, CHP units generation P_g^t, and power from tie line P_{tie}^t.

$$(1+\mu_{\text{eloss}})P^t_{\text{eload}} + P^t_{\text{EB}} = \sum_{g=1}^{N_{\text{G}}} P^t_g + P^t_{\text{w}} + P^t_{\text{tie}}, \tag{21}$$

$$0 \le P^t_{\text{w}} + P^t_{\text{wheat}} \le P^t_{\text{w,avail}}, \tag{22}$$

$$-P^{\max}_{\text{tie}} \le P^t_{\text{tie}} \le P^{\max}_{\text{tie}}, \tag{23}$$

where μ_{eloss} is the electrical power loss coefficient and is set as 0.05 in this paper. $P^t_{\text{tie}} > 0$ means power transfer from the maim grid to the island microgrid, and $P^t_{\text{tie}} < 0$ means the island microgrid transfers redundant power to the main grid. $P^{\max}_{\text{tie}}$ represents the transfer capacity of the tie line. $P^t_{\text{w,avail}}$ is the available wind generation at time t.

3.2.5. Heat Power Balance Constraint

To satisfy the heat demand, a heat power balance needs to be ensured between the total heat load and the heat supply sources, including the CHP units, TES, and EB.

$$Q^t_{\text{EB}} + Q^t_{\text{TES}} + \sum_{g=1}^{N_{\text{G}}} Q^t_g = (1+\mu_{\text{hloss}})P^t_{\text{hload}}, \tag{24}$$

where P^t_{hload} is the heat load at time t. μ_{hloss} is the heat power loss coefficient and set as 0.05 in this paper.

3.2.6. System Reserve Constraint

An amount of power reserve is considered to ensure the power balance against disturbances and contingencies.

$$\sum_{g=1}^{N_{\text{G}}} (P^{\max}_g - P^t_g) \ge R_{\text{e}} * P^t_{\text{eload}}, \tag{25}$$

where R_{e} is the system reserve ratio.

4. Case Study

To validate the effectiveness of the proposed model, a sea island county in China is studied. The island county is located in the northern Yellow Sea on the east side of Liaodong Peninsula and it consists of 195 islands, covering an area of 142 square kilometers on land and 10,324 square kilometers on sea. The sea area has sufficient wind resources and a microgrid system is built to integrate wind generation.

The microgrid consists of 2×20 MW CHP units, 200 MW wind power, and a tie line of 60 MW connecting to the main grid. The prices are set as \$0.06/kWh for wind generation, \$0.5/kWh for the energy transfered through tie line, and \$603/ton for the coal. Tables 1 and 2 illustrate the cost coefficients and technical parameters for the CHP units. Figures 4–6 show a typical daily electrical load profile, a typical daily heat load profile, and the typical available wind power for a month.

Table 1. Cost coefficients of CHP units.

Parameter	Unit	Value
b_0	$\text{t} \cdot \text{h}^{-1}$	4.038
b_1	$\text{t} \cdot (\text{MW} \cdot \text{h})^{-1}$	0.095
b_2	$\text{t} \cdot (\text{MW} \cdot \text{h})^{-1}$	0.014
b_3	$\text{t} \cdot \text{MW}^{-2} \cdot \text{h}^{-1}$	6×10^{-5}
b_4	$\text{t} \cdot \text{MW}^{-2} \cdot \text{h}^{-1}$	1.8×10^{-5}
b_5	$\text{t} \cdot \text{MW}^{-2} \cdot \text{h}^{-1}$	1.3×10^{-6}

Table 2. Technical parameters of CHP units.

$C_{v1,g}$	$C_{v2,g}$	$c_{m,g}$	K_g	P_g^{max}	P_g^{min}	R_g^{up}	R_g^{dn}
0.15	0.15	0.85	−5 MW	20 MW	10 MW	5 MW/h	5 MW/h

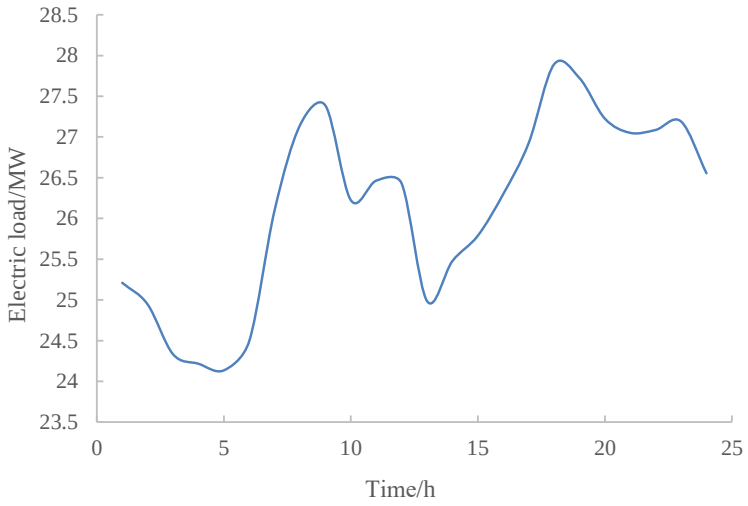

Figure 4. Typical daily electrical load profile.

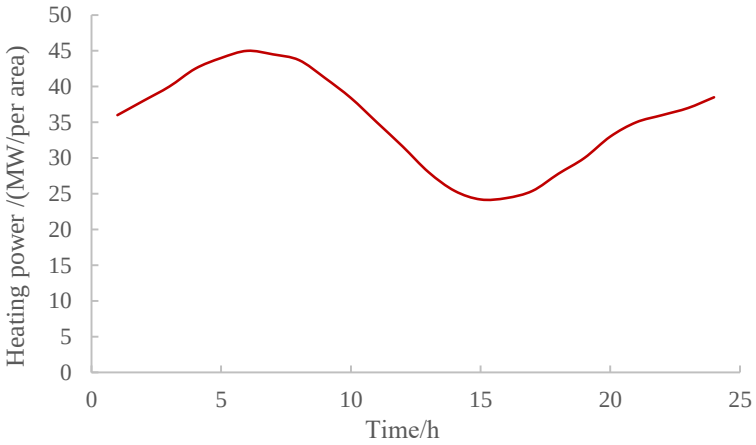

Figure 5. Typical daily heat load profile.

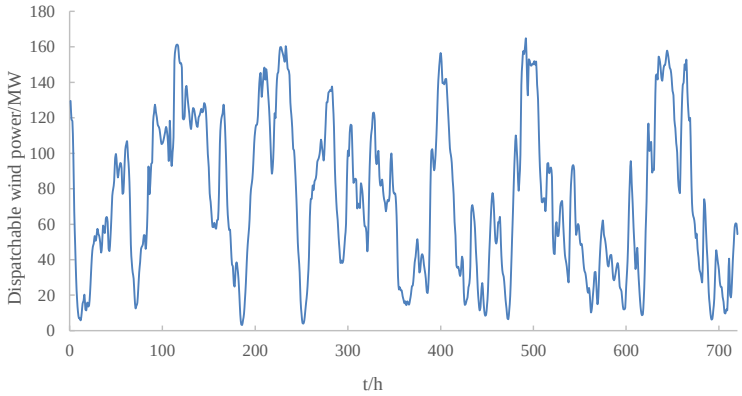

Figure 6. Typical available wind power for a month.

4.1. System Configuration Results

Three cases are tested to analyze the performance of TES and EB in relieving wind curtailment, including (1) without TES and EB, (2) with EB, (3) with TES. The cost of EB is set as $\$4 \times 10^5$ per MW. The efficiencies of TES and EB are set the same as 0.98. Table 3 illustrates the optimal configuration results for the three cases.

Table 3. Configuration results considering TES and EB.

Values	Without EB and TES	With EB	With TES
EB Rated Power Capacity/MW	0	33.53	0
TES Rated Power Capacity/MW	0	0	45.84
TES Rated Energy Capacity/MWh	0	0	328.95
EB Annualized Cost/10^6 \$	0	1.0476	0
TES Annualized Cost/10^6 \$	0	0	1.7166
CHP Generating Cost/10^6 \$	24.5882	24.4054	24.6438
Wind Generation Cost/10^6 \$	8.9750	10.4221	10.7152
Wind Curtailment Penalty/10^6 \$	5.9187	1.8186	0.9880
Tie line Energy Cost/10^6 \$	−80.8849	−80.8849	−82.0155
Wind Power Utilization Rate/%	81.12	94.20	96.85
Total Cost /10^6 \$	−41.4030	−43.1912	−43.9519

As shown in Table 3, the utilization rate of wind power is only 81.12% without any electrical-heat conversion devices. The wind curtailment not only limits the profit of wind turbines (i.e., wind generation cost) to $\$8.975 \times 10^6$ but also leads to a wind curtailment penalty of $\$5.9187 \times 10^6$, which seriously affects the economic performance of wind generation. Taking minimizing the total operating cost as the objective function, the optimal rated power capacity of EB is obtained at 33.53 MW with an annualized cost of $\$1.0476 \times 10^6$. The optimal configuration of TES is obtained as 45.84 MW/328.95 MWh and the annualized cost is $\$1.7166 \times 10^6$.

After installing EB, the utilization rate of wind power increases significantly and reaches 94.20%. As a result, the profit of wind turbine increases to $\$10.4221 \times 10^6$, and the wind curtailment penalty also deceases to $\$1.8186 \times 10^6$. Although there is an additional annualized cost for EB as $\$1.0476 \times 10^6$, the overall annual revenue of the microgrid increases by $\$1.7882 \times 10^6$.

Compared with EB, the installation of TES facilities the bi-direction and time-shifting flexibility support from TES to utilize wind generation. The utilization rate of wind generation further increases to 96.85%. As a result, the wind generation profit increases $\$0.2931 \times 10^6$ compared to the case of installing EB and $\$1.7402 \times 10^6$ compared to the case without EB and TES. The wind curtailment penalty also decreases $\$0.8306 \times 10^6$ and $\$4.9307 \times 10^6$ compared to the other two cases. Although the TES solution requires a higher annualized cost at $\$1.7166 \times 10^6$, the overall annual revenue of the microgrid increases $\$0.7607 \times 10^6$ and $\$2.5489 \times 10^6$ compared to other two cases. It should be noted that the tie line energy profit increases by $\$1.1316 \times 10^6$ when comparing the TES solutions with the EB solution due to the extra bi-direction and time-shifting flexibility.

In summary, comparing the tested three cases, the TES solution realizes a lowest minimum total cost (i.e., highest total revenue), which validates that TES can not only improve the utilization of renewable wind power in the microgrid but also realize a better economic performance.

To further analyze the operational details with the installation of EB and TES, Figure 7 presents the typical two-day power profiles of the available wind power and the utilized wind power with EB. Figure 8 shows the wind power profiles for the same two days after installing TES, and Figure 9 shows the energy states of TES.

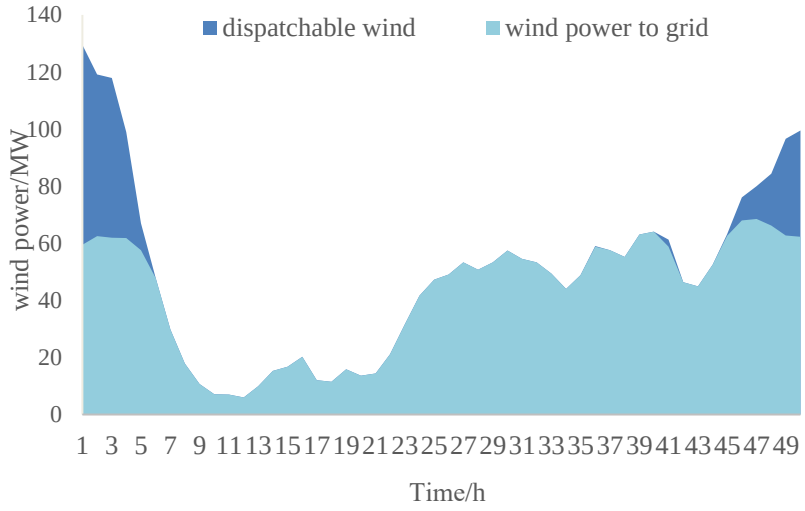

Figure 7. Wind generation with the installation of EB.

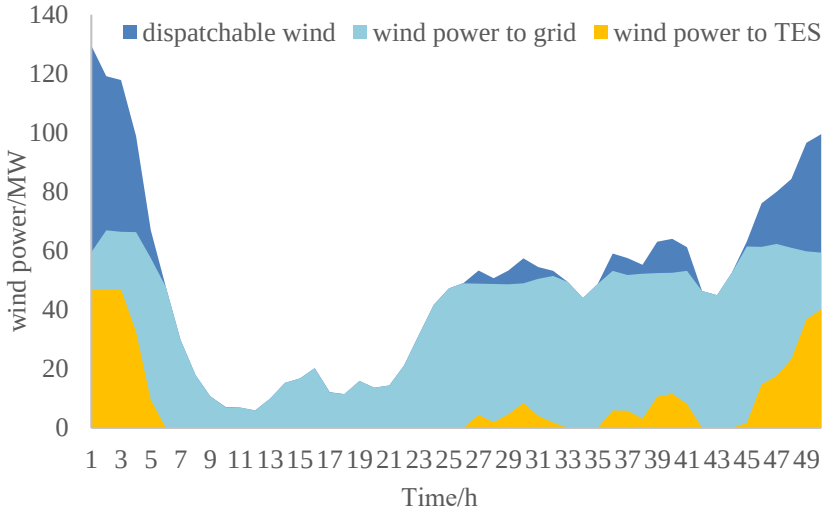

Figure 8. Wind generation with the installation of TES.

As it can be seen from Figures 7 and 8, installing TES can further mitigate the fluctuations of the integrated wind generation compared to installing EB. A part of wind power is stored in TES in heat during the peak period, which realizes peak shaving. The average fluctuation level of wind power can be evaluated by ΔP_{mean} as

$$\Delta P_{\text{mean}} = \frac{1}{T-1} \sum_{t=1}^{T} (|P_{\text{grid}}^{t+1} - P_{\text{grid}}^{t}|). \tag{26}$$

The value of ΔP_{mean} is 6.47 for the original available wind power and it is reduced to 4.65 with the installation of EB. With the configured TES, ΔP_{mean} is reduced to 3.77, which validates that installing TES can increase the utilized wind energy and also smooth the integrated wind power at the same time.

As shown in Figure 9, during hours 1 to 5, TES is in the charging mode due to the surplus wind power and the energy state of TES is also increased. From hour 5 to hour 24, the heating power is decreased due to the reduction of available wind power and the energy state of TES is also declined. The wind power varies during hours 24–44; therefore, the heating power and the energy states of TES are also under fluctuations. After hour 44, the available wind power increases and so as the energy state of TES. In other word, the energy state of TES can reflect the variation of wind power. TES can mitigate the fluctuations of wind power by frequently changing the heating power and storing/releasing thermal

energy to support the power balance of electrical network and increase the utilization rate of wind power.

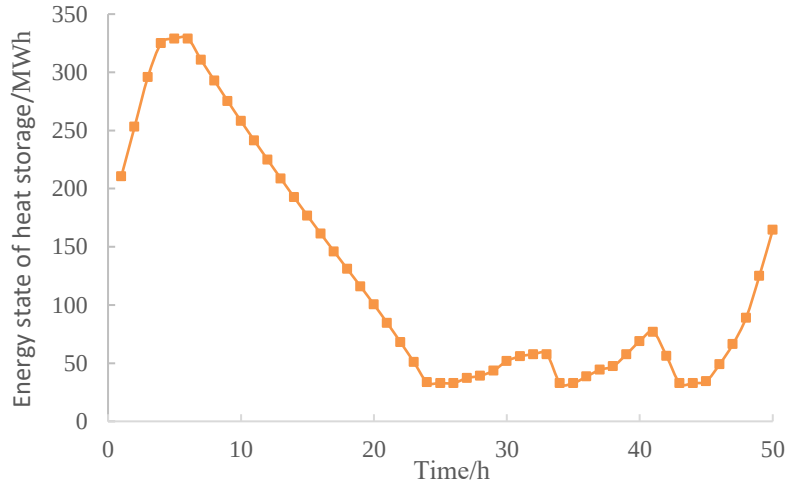

Figure 9. Energy state of TES.

4.2. Performance of TES in Wind Power Utilization under Different Scenarios

The variations of wind power changes along with the months. Figure 10 shows the performance of TES in utilizing wind power with different variation level in different months. The variation level of wind power is represented by the standard deviation of the available wind power. It can be found that the consumption rate of wind power is affected by the variation level. A higher variation level would lead to a lower wind power consumption rate.

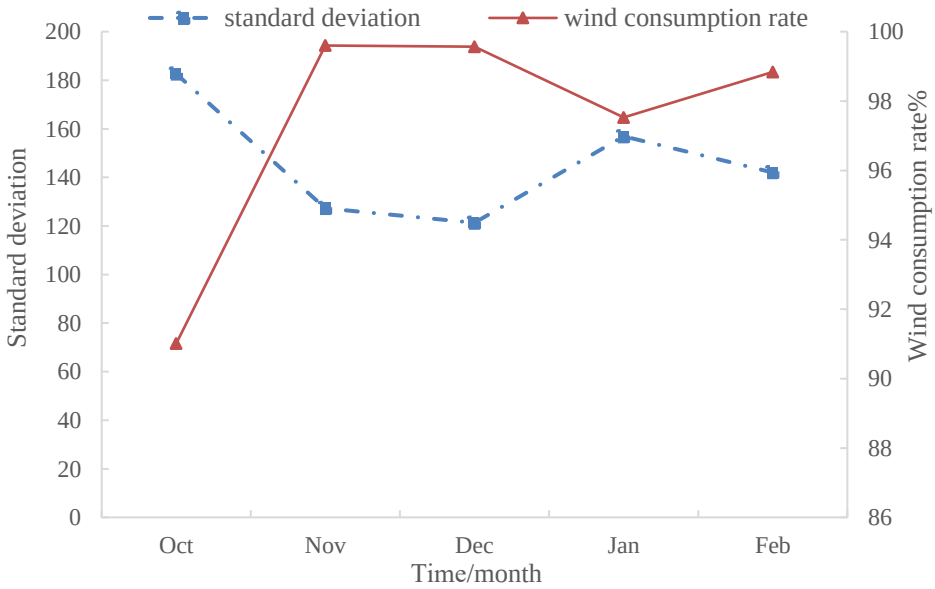

Figure 10. The wind power consumption rates of different months with TES.

The sizing of various components in the microgrid will highly affect the system operational cost and the optimal capacity of TES. The microgrid scale mainly depends on the demand (i.e., electrical load and heat load) and the installed renewable generation. Therefore, a study is performed to discuss the impact of different wind power capacities, different electrical load levels, and different heat load levels on the optimal capacity of TES to achieve the minimum operational cost, as shown in Figures 11–13.

Figure 11 shows the optimal TES configurations and wind consumption rates with different wind power capacities. It shows that a higher capacity of TES is needed for the increased wind power capacity due the increased available wind generation. Moreover, as the electrical load and heat load remain the same in the microgrid, the wind consumption rate will consequently decrease. Therefore, without demand growth in the microgrid, continually installing more wind turbines would lead to an increasing requirement of TES capacity and an declining utilization rate of wind power.

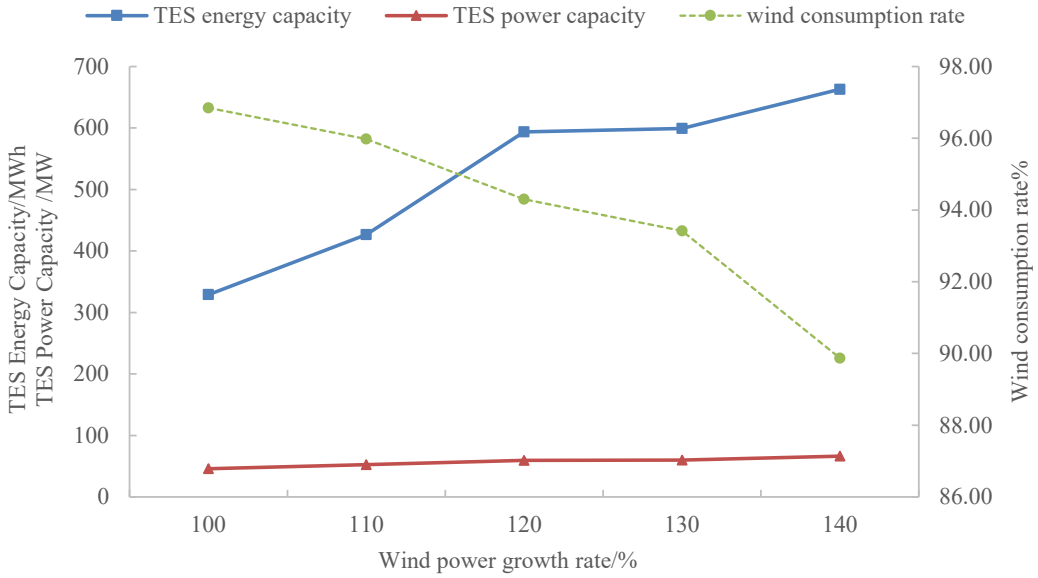

Figure 11. The impact of increased wind power capacity on TES configuration and wind power consumption.

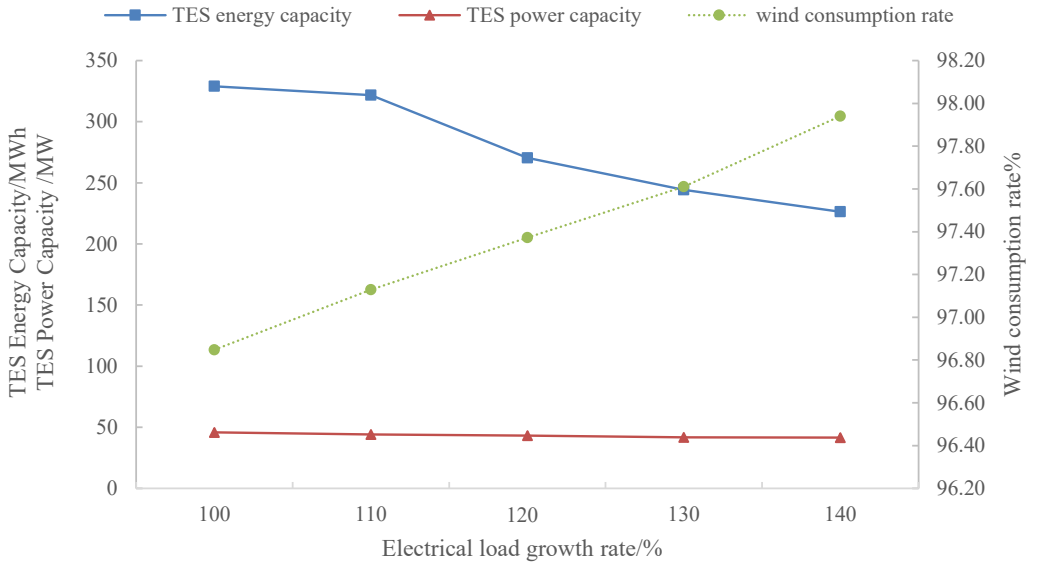

Figure 12. The impact of increased electrical load on TES configuration and wind power consumption.

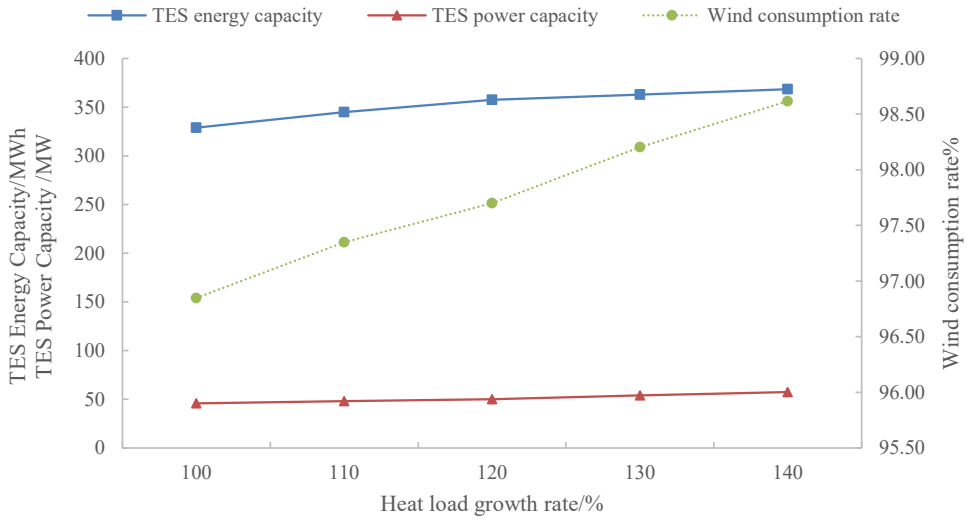

Figure 13. The impact of increased heat load on TES configuration and wind power consumption.

Figure 12 shows the optimal TES capacities and corresponding wind power consumption rates with different electrical load growth rates. The increasing electrical load can consume more wind generation, which leads to a increase in wind power consumption rate. The role of TES in utilizing wind power and supply heat load is reduced accordingly, so the optimal TES capacity is decreased.

Figure 13 shows the optimal TES capacities and corresponding wind power consumption rates with different heat load growth rates. With the increasing heat load, the thermal network can provide more support to wind power utilization. Therefore, a higher optimal TES capacity is obtained accordingly, resulting a stronger capability of utilizing redundant wind energy for heat supply. A wind power consumption rate of 98.59% is realized with 40% growth of heat load.

5. Discussion

Integrating electrical and thermal network can facilitate the regulation capability of thermal network to address the uncertainty in wind generation. CHP units are important components to connect and coordinate the electrical and thermal power. Considering the operating limits of CHP units, introducing additional flexible electricity-heat conversion devices can significantly increase the operational flexibility of the microgrid. As demonstrated in the Case Study, installing EB as an additional resource can not only bring extra profits of wind turbines and reduce the wind curtailment penalty by increasing wind power utilization rate, but also improve the economic performance of the whole microgrid. Moreover, the optimally configured TES can further improve the wind power utilization and increase the economic profits due to its bi-direction and time-shifting flexibility. The additional cost of installing TES can be totally covered by the increased revenue.

Besides, the analyses of TES configurations under different wind power capacities, different electrical load levels, and different heat load levels show that a higher TES capacity is needed for larger wind generation capacity, while the increments in electrical load and heat load can consume more wind generation and provide more flexibility, which leads to less required TES capacity.

6. Conclusions

This paper investigates the optimal configuration of for relieving wind generation curtailment in an island microgrid. By comparing the cases with and without EB and TES, it is found that introducing additional flexible resources to the integrated electricity-thermal microgrid network can bring technical and economic benefits. Further comparisons show that TES can provide better performances in wind power utilization and overall revenue compared to EB due to its additional flexibility. In addition, the analyses of

TES configurations under different scenarios reveal that a microgrid with larger wind generation capacity and lower electrical and heat load demand would require higher TES capacity to achieve the optimal performance.

Author Contributions: Conceptualization, H.L., W.G. and Q.J.; methodology, H.L., J.S., Y.G.; validation, W.G. and Y.G.; formal analysis, J.S.; investigation, H.L.; resources, H.L. and Q.J.; data curation, W.G.; writing—original draft preparation, H.L. and Y.G.; writing—review and editing, H.L., W.G. and Q.J.; visualization, J.S.; supervision, Q.J.; project administration, W.G.; funding acquisition, H.L. and Q.J. All authors have read and agreed to the published version of the manuscript.

Funding: This work was supported in part by the National Key Research and Development Program of China (No. 2019YFB1505400).

Institutional Review Board Statement: Not applicable.

Informed Consent Statement: Not applicable.

Data Availability Statement: The data presented in this study are available on request from the corresponding author. The data are not publicly available due to security and privacy concerns.

Conflicts of Interest: The authors declare no conflict of interest. The funders had no role in the design of the study; in the collection, analyses, or interpretation of data; in the writing of the manuscript, or in the decision to publish the results.

References

1. Cheng, Z.; Geng, G.; Jiang, Q.; Guerrero, J.M. Energy Management of CHP-Based Microgrid with Thermal Storage for Reducing Wind Curtailment. *J. Energy Eng.* **2018**, *144*, 04018066. [CrossRef]
2. Luo, G.L.; Li, Y.L.; Tang, W.J.; Wei, X. Wind curtailment of China's wind power operation: Evolution, causes and solutions. *Renew. Sustain. Energy Rev.* **2016**, *53*, 1190–1201. [CrossRef]
3. Ji, P.; Zhou, X.X.; Wu, S. Review on sustainable development of island microgrid. In Proceedings of the 2011 International Conference on Advanced Power System Automation and Protection, Beijing, China, 16–20 October 2011; Volume 3, pp. 1806–1813. [CrossRef]
4. Ryndzionek, R.; Sienkiewicz, Ł. Evolution of the HVDC Link Connecting Offshore Wind Farms to Onshore Power Systems. *Energies* **2020**, *13*, 1914. [CrossRef]
5. Semero, Y.K.; Zhang, J.; Zheng, D. Optimal energy management strategy in microgrids with mixed energy resources and energy storage system. *IET Cyber-Phys. Syst. Theory Appl.* **2020**, *5*, 80–84. [CrossRef]
6. Tooryan, F.; HassanzadehFard, H.; Collins, E.R.; Jin, S.; Ramezani, B. Smart integration of renewable energy resources, electrical, and thermal energy storage in microgrid applications. *Energy* **2020**, *212*, 118716. [CrossRef]
7. Khorramdel, H.; Aghaei, J.; Khorramdel, B.; Siano, P. Optimal Battery Sizing in Microgrids Using Probabilistic Unit Commitment. *IEEE Trans. Ind. Inform.* **2016**, *12*, 834. [CrossRef]
8. Wang, Y.; Tang, Y.; Xu, Y.; Xu, Y. A Distributed Control Scheme of Thermostatically Controlled Loads for the Building-Microgrid Community. *IEEE Trans. Sustain. Energy* **2020**, *11*, 350–360. [CrossRef]
9. Jing, Z.; Luo, Z. An IGDT Model for Capacity Configuration Optimization of Island Microgrid. *Energy Procedia* **2019**, *158*, 2774–2779. [CrossRef]
10. Li, Y.; Vilathgamuwa, M.; Choi, S.S.; Xiong, B.; Tang, J.; Su, Y.; Wang, Y. Design of minimum cost degradation-conscious lithium-ion battery energy storage system to achieve renewable power dispatchability. *Appl. Energy* **2020**, *260*, 114282. [CrossRef]
11. Zhang, H.; Zhang, Q.; Gong, T.; Sun, H.; Su, X. Peak Load Regulation and Cost Optimization for Microgrids by Installing a Heat Storage Tank and a Portable Energy System. *Appl. Sci.* **2018**, *8*, 567. [CrossRef]
12. Liu, N.; Wang, J.; Wang, L. Hybrid Energy Sharing for Multiple Microgrids in an Integrated Heat–Electricity Energy System. *IEEE Trans. Sustain. Energy* **2019**, *10*, 1139–1151. [CrossRef]
13. Chen, X.; Kang, C.; O'Malley, M.; Xia, Q.; Bai, J.; Liu, C.; Sun, R.; Wang, W.; Li, H. Increasing the Flexibility of Combined Heat and Power for Wind Power Integration in China: Modeling and Implications. *IEEE Trans. Power Syst.* **2015**, *30*, 1848–1857. [CrossRef]
14. Bahramirad, S.; Reder, W.; Khodaei, A. Reliability-Constrained Optimal Sizing of Energy Storage System in a Microgrid. *IEEE Trans. Smart Grid* **2012**, *3*, 2056–2062. [CrossRef]
15. Alipour, M.; Mohammadi-Ivatloo, B.; Zare, K. Stochastic Scheduling of Renewable and CHP-Based Microgrids. *IEEE Trans. Ind. Inform.* **2015**, *11*, 1049–1058. [CrossRef]
16. Alva, G.; Lin, Y.; Fang, G. An overview of thermal energy storage systems. *Energy* **2018**, *144*, 341–378. [CrossRef]
17. Aluisio, B.; Dicorato, M.; Forte, G.; Litrico, G.; Trovato, M. Integration of heat production and thermal comfort models in microgrid operation planning. *Sustain. Energy Grids Netw.* **2018**, *16*, 37–54. [CrossRef]

18. Jin, M.; Feng, W.; Liu, P.; Marnay, C.; Spanos, C. MOD-DR: Microgrid optimal dispatch with demand response. *Appl. Energy* **2017**, *187*, 758–776. [CrossRef]
19. Violante, W.; Cañizares, C.A.; Trovato, M.A.; Forte, G. An Energy Management System for Isolated Microgrids with Thermal Energy Resources. *IEEE Trans. Smart Grid* **2020**, *11*, 2880–2891. [CrossRef]
20. Zhang, G.; Shen, Z.; Wang, L. Online Energy Management for Microgrids with CHP Co-Generation and Energy Storage. *IEEE Trans. Control. Syst. Technol.* **2020**, *28*, 533–541. [CrossRef]